# Analyst

Accepted Manuscript

# Journal Name

## ARTICLE

# A two-photon "turn-on" fluorescent probe based on carbon nanodots for imaging and selective biosensing of hydrogen sulfide in live cells and tissues

Anwei Zhu,[a†] Zongqian Luo,[b†] Changqin Ding,[a] Bo Li,[c] Shuang Zhou,[d] Rong Wang*[b] and Yang Tian*[a]

Determination of hydrogen sulfide ($H_2S$) in live cells and tissues is still a challenge for evaluating the key roles that $H_2S$ plays in the physiological and pathological processes. In this work, a "turn-on" two-photon fluorescent (TPF) sensor for $H_2S$ was developed, in which carbon nanodot (C-Dot) was employed as a two-photon fluorophore due to its large two-photon absorption cross-section ($\sigma$) and AE-TPEA-$Cu^{2+}$ complex [AE-TPEA = N-(2-aminoethyl)-N,N,N'-tris(pyridin-2-ylmethyl)ethane-1,2-diamine] was first designed as a specific receptor for $H_2S$. The fluorescence of C-Dot conjugated with AE-TPEA (C-Dot-TPEA) was quenched upon the addition of $Cu^{2+}$. Then, the fluorescence was restored after the addition of $H_2S$, because $Cu^{2+}$ could be released from TPEA binding site when $H_2S$ interacted with the $Cu^{2+}$ ion. The designed C-Dot-TPEA-$Cu^{2+}$ fluorescent sensor exhibited high specificity for $H_2S$ over biothiols, sulphur-containing compound, reactive oxygen species (ROS), and other biological interferences. Meanwhile, a broad linear range from 5 $\mu M$ to 100 $\mu M$ was obtained and the detection limit was achieved to 0.7 $\mu M$. In addition, the C-Dot-based TPF probe exhibited bright two-photon fluorescence, favourable photo stability against light illumination and pH change, and low cytotoxicity. Accordingly, the nanohybridized TPF sensor with high selectivity and sensitivity, as well as the fascinating properties of C-Dot themselves, successfully provided a new way to TPF imaging and biosensing of $H_2S$ in live cells and tissues. We believe this is the first report of TPF imaging and biosensing of $H_2S$ in live cells and tissues using specially engineered C-Dot-based nanosystem.

## Introduction

Over the past decades, two-photon fluorescent (TPF) probes have attracted much attention for their applications in the field of biomedical imaging and biosensing, because of the low background signal, deep tissue penetration depth, reduced photobleaching, and low phototoxicity associated with the use of near infrared two-photon excitation for TPF probes.[1-5] Recently, carbon nanodot (C-Dot) have emerged as promising TPF probes due to their unique properties such as high water solubility, favourable biocompatibility, and long-term photostability.[6-12] However, exploration of C-Dot for two-photon imaging and sensing still remains at an early stage. In this work, we report the design and synthesis of a two-photon fluorescent probe using C-Dot-based inorganic-organic nanohybrids for imaging and biosensing of physiological hydrogen sulfide ($H_2S$) in live cells and tissues.

Although $H_2S$ is well known for the rotten egg smell, recent studies have demonstrated that $H_2S$ is the third gaseous transmitter, in addition to nitric oxide (NO) and carbon monoxide (CO).[13-14] $H_2S$ contributes to various physiological processes, including relaxation of vascular smooth muscles, mediation of neurotransmission, regulation of inflammation and $O_2$ sensing, and it can also protect against ischemia/reperfusion injury.[15-19] However, disruption of the $H_2S$ level is linked to various diseases such as Alzheimer's disease, Down's syndrome, diabetes, and liver cirrhosis.[20-23]

So far, several elegant techniques have been developed for the detection of $H_2S$, including colorimetric and electrochemical assays, gas chromatography, and metal-induced sulfide precipitation.[24-30] Fluorescence imaging and biosensing with spatial or temporal resolution for typical cell-based or live tissue experiments have attracted great attention in recent years.[31-38] However, most of fluorescent probes for $H_2S$ have been evaluated using one-photon microscopy and require relatively short excitation wavelengths,[31-35] limiting their use in deep-tissue imaging because of the shallow penetration depth (<80 $\mu m$). Besides, the design and synthesis of new TPF probes from small molecules with suitable water solubility, biocompatibility and photostability is still very challenging.

Herein, we develop a TPF "turn-on" fluorescent sensor for $H_2S$ with high selectivity and sensitivity, in which C-Dot was

employed as a TPF fluorophore and AE-TPEA/Cu²⁺ complex (AE-TPEA= *N*-(2-aminoethyl)-*N*,*N*,*N′*-tris(pyridin-2-ylmethyl)ethane-1,2-diamine) was designed as a specific receptor for H₂S. In our previous work, AE-TPEA was used as a recognition element for Cu²⁺ and AE-TPEA/Cu²⁺ showed high stability in the presence of biological metal ions and amino acids.[39-40] As illustrated in Scheme 1, the fluorescence of C-Dot conjugated with AE-TPEA (C-Dot-TPEA) was quenched upon the addition of Cu²⁺. Then, as expected, the fluorescence was restored after the addition of H₂S, because Cu²⁺ could be released from the AE-TPEA/Cu²⁺ complex when H₂S bond to the Cu²⁺ center. The designed C-Dot-TPEA-Cu²⁺ fluorescent sensor demonstrated high selectivity for H₂S over other potential interferences. Furthermore, the present biosensor showed a broad linear range of 5–100 μM and a low detection limit of 0.7 μM. Finally, the significant analytical performance of the biosensor, as well as good photo stability and low cytotoxicity of C-Dot, established a reliable fluorescent probe for TPF imaging and biosensing of H₂S in live cells.
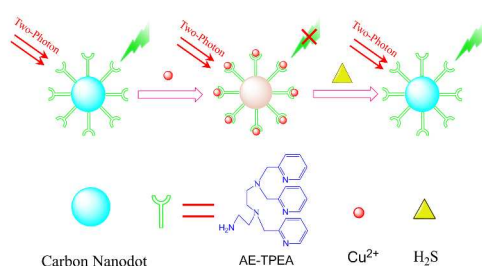


**Fig. 1** Working principle of the C-Dot-TPEA-Cu²⁺ fluorescent probe for H₂S detection.

## Experimental

### Reagents and chemicals

Graphite rods were purchased from Alfa Aesar. Methanol, ethanol, dichloromethane, petroleum ether, ethyl acetate, acetonitrile, diethyl ether, tetrahydrofuran, L-Glutathione (GSH), L-cysteine (L-Cys), DL-Homocysteine (DL-Hcy), 2-mercaptoethanole (2-ME), dithiothreitol (DTT), metal salts, and silica gel (200-300 meshes) were obtained from Sinopharm. Sodium sulfite (Na₂SO₃), sodium thiosulfate (Na₂S₂O₃), and Triton X-100 were obtained from Aladdin. Sodium sulfide nonahydrate (Na₂S·9H₂O), N-hydroxysuccinimide (NHS), 1-Ethyl-3-(3-dimethylaminopropyl)carbodiimide (EDC), methyl thiazolyl tetrazolium (MTT), ethylenediamine (99%), chloroform-d (99.8%), and N-(2-bromoethyl)phthalimide, 2,2-Azobis (2-amidinopropane) dihydrochloride (AAPH) were purchased from Sigma-Aldrich. Hydrazine hydrate was obtained from TCI AMERICA. Cell culture media and supplements were supplied by Invitrogen Corporation. Annexin V-FITC Apoptosis Assay Detection Kit was purchased from KeyGEN Biotech. Ultrapure water was used from a Millipore water purification system. Superoxide anion (O₂·⁻) was chemically generated by the reaction between hydrogen peroxide (H₂O₂, 10 mM) and cerium sulfate (Ce(SO₄)₂,100 mM). Hydroxyl radical (HO·) was generated by the Fenton reaction (0.1 mM H₂O₂ and 0.6 mM Feᴵᴵ(EDTA)). Alkyl peroxyl radical (ROO·) was generated by thermolysis of AAPH (10 mM) in air-saturated aqueous solution at 310 K. Singlet oxygen (¹O₂) was generated as a product of the disproportionation of H₂O₂ (20 mM) in alkaline solution

(pH=10) catalyzed by molybdate ions (20 mM).[41-44] NO was released from the agent *S*-nitroso-*N*-acetyl-ᴅ,ʟ-penicillamine.[45] HNO was chemically generated in buffered aqueous solution treated with Angeli's salt.[46]

### Preparation of C-Dot

C-Dot was synthesized according to the previously reported electrochemical method.[6,39-40,47] Briefly, 0.3 g NaOH was dissolved in 100 mL ethanol/H₂O (99.5:0.5, v:v). By using graphite rods (diameter of 0.5 cm) as both anode and cathode, C-Dot was obtained at a current intensity of 40 mA cm⁻² for 12 h. The raw C-Dot solution was treated with a suitable amount of MgSO₄ (5–7 wt%) and stirred for 20 min. Then, it was left to stand for 24 h to remove the salts and water. Afterwards, the ethanol in the purified C-Dot solution was removed by vacuum distillation. To introduce carboxyl groups on the surface of C-Dot, the aqueous C-Dot solution was mixed with concentrated nitric acid, and the mixture was heated at reflux for 24 h. The excessive acid was finally neutralized by NaOH and then removed by dialyzing against Milli-Q water.

### Synthesis of AE-TPEA

*N*,*N*,*N′*-tri(pyridine-2-ylmethyl)ethane-1,2-diamine (TPEA) was first synthesized using a modified literature procedure.[48-51] Then, TPEA (4.31g, 12.9 mmol), N-(2-bromoethyl)phthalimide (3.28 g, 12.9 mmol), anhydrous K₂CO₃ (4 g, 28.9 mmol), and KI (0.215 g, 1.29 mmol) were mixed in 40 mL of CH₃CN, the reaction was stirred at reflux for 24 h under nitrogen atmosphere. Concentration and purification of the obtained brown oil by basic alumina column chromatography (a mixture of CH₂Cl₂-CH₃OH as eluent) produced a tan solid. Next, to its solution in anhydrous ethanol (35 mL) was added hydrazine hydrate (0.625 mL, 12.9 mmol). After the product was cooled to room temperature, HCl (10.8 mL, 129 mmol) were added and the mixture was stirred for another hour at room temperature. The white solids were filtered off and the ethanol was removed by vacuum distillation. To this aqueous mixture was added NaOH. The aqueous phase was extracted three times with CH₂Cl₂ and the combined organic layers were dried over Na₂SO₄, filtered, and the solvent was removed, resulting in the product (N-(2-aminoethyl)-N,N',N'-tris(pyridine-2-ylmethyl)ethane-1,2-diamine, AE-TPEA) as a brown oil. Yield=40%. ¹H NMR (400 MHZ, CDCl₃): 8.53~8.48 (m, 3H, C₅H₄N), 7.64~7.10 (m, 9H, C₅H₄N), 3.81 (m, 4H, CH₂), 2.72~2.67 (m, 6H, CH₂CH₂), 2.51 (t, 2H, CH₂CH₂), 1.60 (br, 2H, NH₂). ¹³C NMR (100 MHZ, CDCl₃): δ 160.0, 159.6, 148.9, 148.8, 136.3, 136.2, 122.8, 122.7, 121.9, 121.8, 66.0, 60.8, 57.8, 52.5, 52.3, 39.7. TOF MS EI⁺: calculated for [M+H]⁺ 376.2375, found 376.2377.

### Preparation of C-Dot-TPEA

EDC/NHS (20 mM) and AE-TPEA (2 mM) were added into the obtained C-Dot solution and stirred for ~2 h. Finally, the nanohybrids were separated from the free EDC/NHS and AE-TPEA molecules by three cycles of concentration/dilution (10:1), using a Nanosep centrifugal device (Pall Corporation, MW cutoff of 3 kDa), and re-dispersed in PBS buffer (pH=7.4).

### Instruments and methods

Optical absorption spectra were recorded by an Agilent 8453 UV-vis-NIR spectrophotometer. Infrared spectroscopic data were collected by infrared spectrometer (AVATAR-370DTGS).

In order to observe the morphology of C-Dot, transmission electron microscopy (HR-TEM, JEOL 2100, Japan) was employed. X-ray photoelectron spectroscopy (XPS) was carried out by PHI-5000C ESCA system (Perkin Elmer) with Mg $K_\alpha$ radiation (hv=1253.6 eV). All binding energies (BEs) were referred to as the C 1s peak (284.6 eV) arising from surface hydrocarbons (or adventitious hydrocarbon). AFM images were recorded by Picoscan 2100 MI, USA. One-photon fluorescence spectra were obtained on a VARIAN Cary-Eclipse 500 fluorescence spectrophotometer. Two-photon spectra were recorded on a spectrometer (HORIBA Model iHR550) and the pump laser beam came from a mode-locked Ti: sapphire laser system (Coherent Mira900). The cell images were taken by a confocal laser scanning microscope (Leica TCS SP8) equipped with a mode-locked Ti: sapphire laser source (Mai Tai DeepSee, 80 MHz, ~90 fs).

### Cell culture and cytotoxicity assay

Cells were cultured in Dulbecco's Modified Eagle's medium (DMEM) containing high glucose supplemented with fetal bovine serum (10 %, v/v), penicillin (100 units mL$^{-1}$), and streptomycin (100 µg mL$^{-1}$). The cellular cytotoxicity of C-Dot-TPEA-Cu$^{2+}$ was tested by means of a standard MTT (methyl thiazolyl tetrazolium) assay. Firstly, the cells (~$3\times10^5$ cells mL$^{-1}$) were seeded onto a 96-well microliter plate in an atmosphere of 5 % CO$_2$ and 95 % air at 310 K humidified incubator for 48 h. Then, the cells were incubated in the fresh culture medium containing the C-Dot-TPEA-Cu$^{2+}$ with different concentrations for 48 h. Thereafter, 100 µL of the new culture medium containing MTT (10 µL, 5 mg mL$^{-1}$) was added to each well followed by incubation for 4 h to allow the formation of formazan dye. Finally, the supernatant was removed before 150 µL of DMSO was added to each well and the plate was shaken for 10 min. By measuring the absorbance at 490 nm in a Multiskan MK3 microplate photometer (Thermo Scientific), the cell viability values were determined (at least 3 times) according to the following formula: cell viability (%) = the absorbance of experimental group/the absorbance of blank control group × 100%.

### Apoptosis assay

HeLa cells were incubated with C-Dot-TPEA-Cu$^{2+}$ at concentrations of 0.02, 0.06, 0.10 mg mL$^{-1}$ for 24 h. Cells floating in the cell medium were collected by centrifuge while adherent cells were collected by treating with trypsin-EDTA. After washing with PBS, cells were then stained with FITC-annexin V (Molecular Probe) and Propidium Iodide (PI, Aldrich) following the standard protocol. A Becton-Dickinson flow cytometer was used for the flow cytometry measurements.

### In vitro fluorescence imaging

Firstly, one day before imaging studies, the cultured cells were passaged and plated on a Petri dish. The culture media was replaced with 1 × PBS (pH=7.4) containing the C-Dot-TPEA probes, and the cells were incubated for ~1 h at 310 K. The cells were washed with 1 × PBS (pH=7.4) three times. The fluorescence imaging of HeLa cells were obtained with a spectral confocal and multiphoton microscopes (Leica TCS SP8). One-photon fluorescence images were obtained with an excitation wavelength at 488 nm and a collection window in the 520-700 nm range, and two-photon fluorescence images were excited at 800 nm and collected in the 440-650 nm range Then,

100 µM CuCl$_2$ were added and further incubated for ~1 h before imaging. Finally, 50 and 100 µM Na$_2$S were added and incubated with cells for ~30 min, and then fluorescence images were acquired.

### Preparation and staining of lung cancer tissue slices

Tissue slices were prepared from the human lung cancer A549 cells. A total of $2\times10^6$ A549 cells diluted in 200 µL of serum-free DMEM medium were injected subcutaneously into the right flank of 6 to 8-week-old BALB/c nude mice to inoculate tumors. On day 15 after A549 inoculation, mice were sacrificed. Tumors were removed and embedded with O.C.T (Sakura Finetek, USA, Torrance, CA) for frozen sections. The tissues were cut into 250 µm-thick slices using a vibrating-blade microtome. Slices were treated with C-Dot-TPEA nanoprobe (0.2 mg mL$^{-1}$) for 6 h at 310 K, then with CuCl$_2$ (500 µM) for 1 h, and Na$_2$S (500 µM) for ~30 min. The slices were washed three times with 1×PBS and transferred to slice boxes for observation. The two-photon microscopy images of lung cancer tissue slices labeled with the nanoprobe were obtained at depths of 90–180 µm.

## Results and discussion

### Characterization of C-Dot-TPEA probe

The C-Dot was synthesized according to the previously reported electrochemical method.[6,39-40,47] A typical transmission electron microscopy (TEM) image (Fig. 2A) shows that the as-synthesized C-Dot is ~5 nm in size. The corresponding atomic force microscopy (AFM) image (Fig. 2B, top) revealed a typical topographic height of 4.7−5.2 nm (Fig. 2B, bottom), suggesting that the average thickness of C-Dot is ~5 nm. The infrared (IR) spectrum of the C-Dot is given in Fig. 2C. The peaks located at ~2973 and 1563 cm$^{-1}$ correspond to the C=C stretch of polycyclic aromatic hydrocarbons. The peak observed at ~1666 cm$^{-1}$ indicates the existence of carbonyl (C=O) groups, while the band at ~3405 cm$^{-1}$ is ascribed to the OH stretching
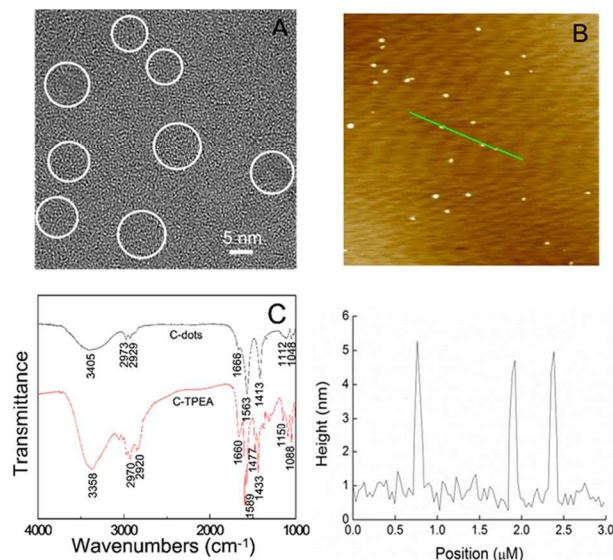


**Fig. 2** (A) TEM image of the C-Dot; (B) (top) AFM topography image of C-Dot on silicon substrate with (bottom) the height profile along the green line in the topographic image; (C) FTIR spectra of the as-prepared C-Dot and C-Dot-TPEA.

mode. These data demonstrate that the as-synthesized C-Dot was surrounded by –COOH and/or –OH groups.

On the other hand, AE-TPEA was designed and synthesized by substituting TPEA with N-(2-bromoethyl)phthalimide in acetonitrile followed by deprotection of the product with hydrazine hydrate. Then, AE-TPEA molecules were conjugated with C-Dot by using EDC and NHS as catalysts. The modification process of AE-TPEA on the C-Dot was tracked by IR spectroscopy and X-ray photoelectron spectroscopy (XPS, Supporting Information (SI), Fig. S5). As shown in Fig. 2C, the peak obtained at ~1660 $cm^{-1}$ indicates the existence of carbonyl (C=O) groups, while the band located at ~1477 $cm^{-1}$ is ascribed to the bending vibration of the -NH group. The peak observed at ~3358 $cm^{-1}$ corresponds to the –NH stretching. The result demonstrated the formation of new amide group on the C-Dot surface. In addition, two peaks ascribed to N 1s were observed in XPS after the modification of AE-TPEA on the C-Dot surface (SI, curve b in Fig. S5). The first peak located at ~399.1 eV is attributed to the pyridinic nitrogen-type. The second peak observed at ~401.5 eV is interpreted as nitrogen from amide group. The XPS results confirm the successful modification of AE-TPEA on the C-Dot surface.

As shown in Fig. 3 (curve a), the UV-Vis absorption peak of the C-Dot at 250–300 nm represents a typical absorption of an aromatic π system.[47] The fluorescence intensity of the C-Dot is strong enough to be easily seen with the naked eye. Upon excitation at 400 nm, the bare C-Dot show a strong emission at 495 nm as demonstrated in Fig. 3 (curve b). The two-photon fluorescence spectrum was a little red shift, compared with one-photon fluorescence spectrum (curve c and b). Using rhodamine B as a standard, the fluorescence quantum yield ($\Phi$) of C-Dot was calculated to be about 10%. In addition, the two-photon absorption cross-section (σ) of C-Dot was estimated by determining the two-photon luminescence intensities of the specimen and a reference under the same experimental conditions. By using rhodamine B as the reference, the σ value for the C-Dot at 800 nm was estimated to be 32000 ± 4000 GM (Goeppert-Mayer unit, with 1 GM = $10^{-50}$ $cm^4$ s/photon). The result is comparable with that for the two-photon C-Dot prepared by a different method and those for other two-photon luminescent nanomaterials including CdSe and CdSe/ZnS.[2,6-10,38] The high σ value for the C-Dot should be very benefit for two-photon imaging and biosensing in live cells, deep tissues, and animals.
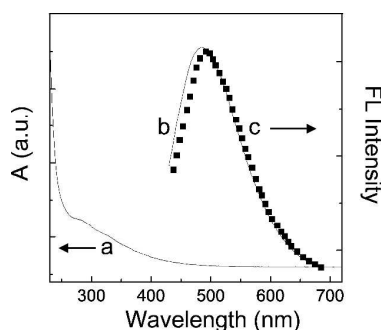


**Fig. 3** (a) UV-vis absorption spectrum, (b) one-photon (400 nm excitation) and (c) two-photon (800 nm excitation) fluorescence spectra of the as-prepared C-Dot.

### One-photon and two-photon detection of H₂S

The fluorescent $Cu^{2+}$ titration in the C-Dot-TPEA solution (0.04 mg $mL^{-1}$) was first performed upon one-photon excitation (taking account of the further cell experiments, 488 nm was

selected as the excitation wavelength). As shown in Fig. 4A, the fluorescence in the 500–700 nm range shows continuous quenching with the addition of $Cu^{2+}$. The fluorescent peak intensity ($\lambda_{em}$ = 560 nm) has a good linearity with the concentration of $Cu^{2+}$ in the range of 5–100 μM (Fig. 4B). As expected, upon the addition of $Na_2S$ (a commonly employed $H_2S$ donor),[52-53] emission turn-on with a little red shift is clearly observed (Fig. 4C). Moreover, the fluorescent peak intensity is in a good linearity with the concentration of $Na_2S$ in the range of 5−100 μM (Y=6.5789X+185.2631, $R^2$=0.9928, Fig. 4D).
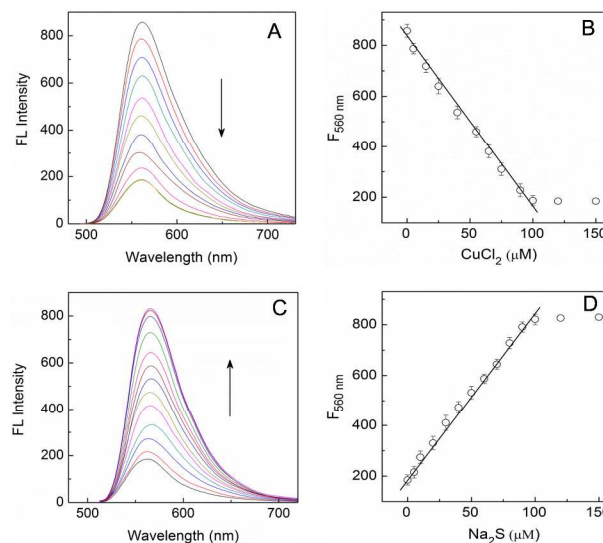


**Fig. 4** (A) One-photon fluorescence spectra of C-Dot-TPEA (0.04 mg $mL^{-1}$) upon addition of different concentrations of $Cu^{2+}$ ions (0–150 μM) in phosphate buffer solution (PBS, pH 7.4). Excitation wavelength: 488 nm; (B) Plot of fluorescent peak intensity at 560 nm of C-Dot-TPEA with the addition of $Cu^{2+}$; (C) One-photon fluorescence spectra of the mixture of C-Dot-TPEA (0.04 mg $mL^{-1}$) and $Cu^{2+}$ (100 μM) upon addition of different concentrations of $Na_2S$ (0–150 μM) in PBS (pH 7.4). Excitation wavelength: 488 nm; (D) Plot of fluorescent peak intensity of the C-Dot-TPEA-$Cu^{2+}$ in the presence of increasing $Na_2S$ concentrations. These experiments were repeated three times.

On the other hand, under two-photon excitation at 800 nm, the fluorescent intensity in the 440–650 nm range gradually decreases with increasing the concentration of $Cu^{2+}$ as shown in Fig. 5A. The fluorescent peak at 495 nm gives a good linearity with the concentration of $Cu^{2+}$ in the range of 5–100 μM as plotted in Fig. 5B. Similar to that upon one-photon excitation, the fluorescence can be obviously restored upon the addition of $Na_2S$ (Fig. 5C). The CuS precipitate with large reflection and scattering which could be generated in the reaction between $H_2S$ and C-Dot-TPEA-$Cu^{2+}$ may contribute to the red shift of the fluorescent peak. The two-photon fluorescent peak intensity at 500 nm varied linearly with the concentration of $Na_2S$ in the range of 5–100 μM (Y=12.2500X+657.5000, $R^2$=0.9897, Fig. 5D), which meets the requirement for the detection of $H_2S$ in the biological system.[53-57] The detection limit was estimated to be 0.7 μM (based on a signal-to-noise ratio of S/N=3). Meanwhile, the reaction between C-Dot-TPEA-$Cu^{2+}$ and $H_2S$ was observed to be complete in ~200 s (SI, Fig. S6).

### Selectivity, stability, and cytotoxicity

The complexity of bioimaging and biosensing in live cells presents a great challenge to the analytical methods not only in sensitivity, but more importantly in selectivity. The selectivity

for $H_2S$ was demonstrated by the fluorescence changes ($\Delta F1$) induced by potential interferences over the fluorescence changes by $H_2S$ ($\Delta F$). Firstly, various thiols (5 mM GSH or 0.5 mM L-Cys, DL-Hcy, 2-ME, and DTT), as well as sulphur-containing compounds (1 mM $Na_2SO_3$, $Na_2S_2O_3$, and KSCN), were examined. Remarkably, as shown in Fig. 6A (white bars), negligible fluorescence changes (<5%) are observed for both thiols and sulphur-containing compounds at higher concentrations, compared with that for 100 μM $H_2S$. In addition, the fluorescent probe C-Dot-TPEA-$Cu^{2+}$ did not show obvious fluorescence enhancement in response to reactive oxygen species (1 mM $O_2\cdot^-$, $H_2O_2$, $OCl^-$, $HO\cdot$, $ROO\cdot$ and $^1O_2$), nitrogen oxides (0.1 mM for NO and HNO) or ascorbic acid (AA, 5 mM). Moreover, these potential interferences including thiols, sulphur-containing compounds, ROS, NO, HNO and AA showed negligible effects on the fluorescent signal for $H_2S$ sensing (Fig. 6A, black bars). The high selectivity of the present biosensor for $H_2S$ should be ascribed to the specific affinity of the designed C-Dot-TPEA-$Cu^{2+}$ toward $H_2S$.
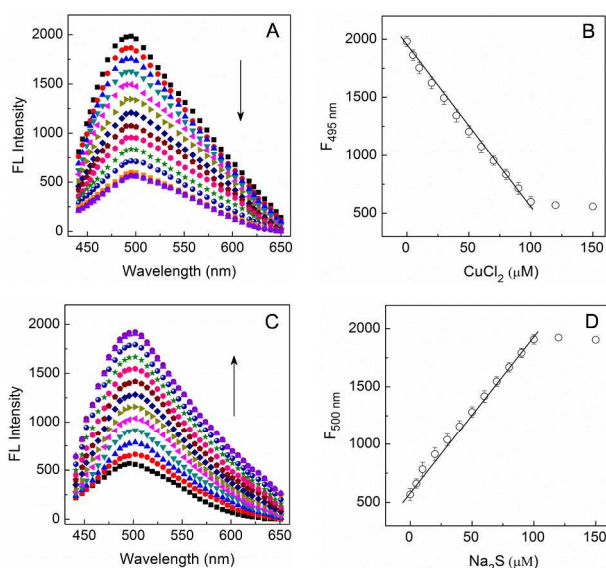


**Fig. 5** (A) Two-photon fluorescence spectra of C-Dot-TPEA (0.04 mg mL$^{-1}$) upon addition of different concentrations of $Cu^{2+}$ (0–150 μM) in PBS (pH 7.4). Excitation wavelength: 800 nm; (B) Plot of fluorescence intensity at 495 nm of C-Dot-TPEA with the addition of $Cu^{2+}$; (C) Two-photon fluorescence spectra of the mixture of C-Dot-TPEA (0.04 mg mL$^{-1}$) and $Cu^{2+}$ (100 μM) upon addition of different concentrations of $Na_2S$ (0–150 μM) in PBS (pH 7.4). Excitation wavelength: 800 nm; (D) Plot of fluorescence intensity at 500 nm of the C-Dot-TPEA-$Cu^{2+}$ in the presence of increasing $Na_2S$ concentrations. These experiments were repeated three times.

Significantly, the as-prepared C-Dot-based fluorescent probe which can freely disperse in water with transparent appearance exhibited good photostability. As shown in Fig. 6B, negligible changes (<5%) of the fluorescent intensity can be obtained up to 2 h under continuous excitation at 800 nm. Moreover, no significant fluorescence changes for the C-Dot-TPEA-$Cu^{2+}$ probe are observed over the biologically relevant pH range from 5.0 to 9.0 (Fig. 6C). These results indicate that superior to organic dyes, the C-Dot-based probe demonstrated excellent stability against light illumination, pH variation, and air condition, which would be very benefit for imaging and biosensing in live cells and other biological environments.

For further biological application point of view, MTT assays were carried out to evaluate the cytotoxicity of the C-Dot-based

probe to HeLa, RAW264.7 and HEK 293T cells. As expected, the viability of both normal cells and cancer cells declined only by < 9% after their incubation with 0.10 mg mL$^{-1}$ fluorescent probes for 48 h at 37 °C (Fig. 6D). Thus, the as-prepared C-Dot-TPEA-$Cu^{2+}$ probe can be considered to be low toxic for the $H_2S$ detection in live cells.
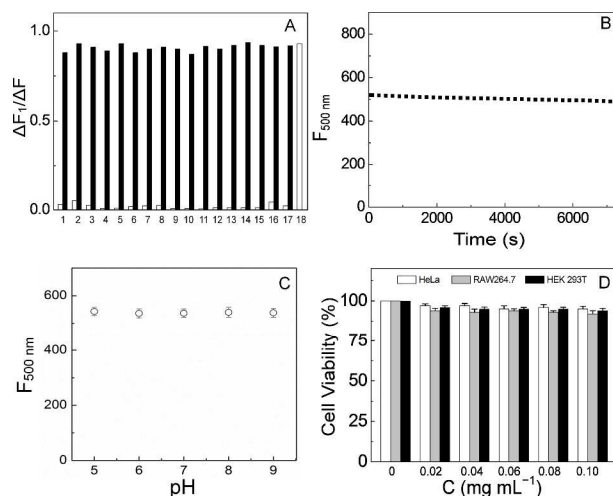


**Fig. 6** (A) Fluorescence responses of the C-Dot-TPEA solution (0.04 mg mL$^{-1}$) containing $Cu^{2+}$ (100 μM) in PBS (pH 7.4) after the addition of thiols, sulphur-containing compounds, and ROS (1-18: 1, GSH; 2, Cys; 3, Hcy; 4, 2-ME; 5, DTT; 6, $SO_3^{2-}$; 7, $S_2O_3^{2-}$; 8, SCN$^-$; 9, $O_2\cdot^-$; 10, $H_2O_2$; 11, OCl$^-$; 12, HO$\cdot$; 13, ROO$\cdot$; 14, $^1O_2$; 15, NO; 16, HNO; 17, AA; 18, $S^{2-}$). The white bars represent the addition of various thiols (5 mM for GSH, 0.5 mM for Cys, Hcy, 2-ME, and DTT), sulphur-containing compounds (1 mM for $Na_2SO_3$, $Na_2S_2O_3$, KSCN), ROS (1 mM for $O_2\cdot^-$, $H_2O_2$, OCl$^-$, HO$\cdot$, ROO$\cdot$, $^1O_2$), nitrogen oxides (0.1 mM for NO, HNO), AA (5 mM) or $Na_2S$ (100 μM). The black bars represent the subsequent addition of 100 μM $Na_2S$ to the above solution; (B) The fluorescence intensity of C-Dot-TPEA-$Cu^{2+}$ (0.1 mg mL$^{-1}$) as a function of time measured with 3 min intervals ($\lambda_{ex}$ = 800 nm, $\lambda_{em}$ = 500 nm); (C) Effect of pH value on the fluorescent responses of C-Dot-TPEA-$Cu^{2+}$ (0.1 mg mL$^{-1}$); (D) Cell viability values (%) estimated by MTT proliferation test versus concentrations of C-Dot-TPEA-$Cu^{2+}$ after 48 h incubation at 37 °C. Three cell lines, HeLa, RAW264.7 and HEK 293T, were cultured in the 0.02–0.10 mg mL$^{-1}$ C-Dot-TPEA-$Cu^{2+}$ solutions at 37 °C for 48 h, respectively.

Next, apoptosis assay were carried out to confirm the biocompatibility of C-Dot-TPEA-$Cu^{2+}$ by flow cytometry (FACS) measurements. Taking HeLa cells as an example, they were first incubated with C-Dot-TPEA-$Cu^{2+}$ at concentrations of 0.02, 0.06, and 0.10 mg mL$^{-1}$ for 24 h. Then, the cells were stained by FITC-annexin V and Propidium iodide (PI) to label the apoptosis cells and necrotic cells respectively for FACS measurement (SI, Fig. S7). It is demonstrated that the C-Dot-TPEA-$Cu^{2+}$ probes have good biocompatibility to HeLa cells.

Moreover, to investigate the photo-toxicity associated with laser irradiation, HeLa cells were first irradiated at 800 nm for 1 h by a femtosecond laser. From the bright-field images of HeLa cells (SI, Fig. S8), no obvious changes were observed before and after the irradiation. Then, to determine the health of HeLa cells after irradiation, a standard live/dead staining procedure using commercially available propidium iodide (PI) was further performed.[58] As shown in the inset of Fig. S8B (SI), when the irradiation-pretreated HeLa cells were incubated with PI, to which they are normally impermeable, no intracellular fluorescence signal at 620 ± 20 nm was observed in the confocal fluorescence imaging. This confirmed that the PI hardly crossed the cell membrane, and that the irradiation-pretreated HeLa cells were normal healthy cells.

### One- and two-photon imaging of H$_2$S in live cells and tissues

As demonstrated above, the advantages of high selectivity and sensitivity, together with small size, remarkable stability against illumination and pH, and especially good biocompatibility of C-Dot-based fluorescent probe substantially provide a reliable platform for TPF bioimaging and biosening application. Herein, to demonstrate its competence in monitoring the change of H$_2$S in HeLa cells, C-Dot-TPEA probes were first incubated with HeLa cells for ~1 h and then washed with 1×PBS (pH 7.4). Strong fluorescence images were observed upon 488 nm (one-photon, Fig. 7A) and 800 nm (two-photon, Fig. 7G) excitation. The overlay of fluorescence and bright-field channel reveals that the fluorescent signals were localized in the perinuclear region of the cytosol (Fig. 7B and 7H), indicating the excellent cell permeability of the C-Dot-TPEA probe. As expected, the fluorescence intensities obviously decreased after the incubation of cells with CuCl$_2$ (100 μM) for ~1 h at 310 K upon one- (Fig. 7C) or two-photon (Fig. 7I) excitation. Next, Na$_2$S (50 μM and 100 μM) was added to the medium, a large intracellular fluorescence enhancement was observed under either one-photon (Fig. 7D and 7E) or two-photon condition (Fig. 7J and 7K). The fluorescence emission changes after the addition of different molecules were quantified and summarized in Fig. 7F (one-photon) and Fig. 7L (two-photon). Analogous studies in RAW264.7 and HEK 293T cells show similar results (SI, Fig. S9).

Then, we further investigated the utility of this two-photon fluorescence probe in tissues imaging. The two-photon fluorescence and bright-field images (Fig. 8A and 8B) show that the C-Dot-TPEA probe was evenly distributed in the lung cancer tissue slice. Furthermore, the two-photon excited fluorescence in lung cancer tissue slice was quenched upon addition of Cu$^{2+}$ (Fig. 8C), suggesting that the C-Dot-TPEA probes response to Cu$^{2+}$ sensitively. Then, after the addition of Na$_2$S, the fluorescence was restored as shown in Fig. 8D. In addition, the two-photon fluorescence imaging along the z-direction (SI, Fig. S10) demonstrated that the C-Dot-TPEA-Cu$^{2+}$ probe was capable of monitoring H$_2$S changes at depth of 90–150 μm in living tissues using two-photon microscopy.
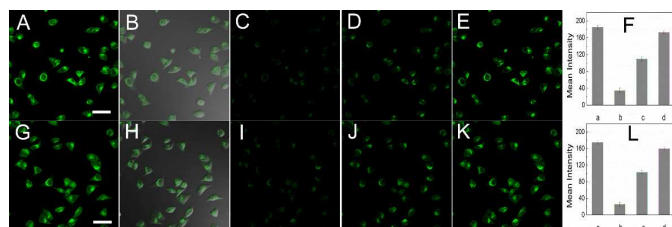


**Fig. 7** (A, G) The fluorescence images and (B, H) the overlay of fluorescence and bright-field images of HeLa cells incubated with 0.04 mg mL$^{-1}$ C-Dot-TPEA for ~1 h upon (A, B) 488 nm and (G, H) 800 nm excitation; (C, I) The fluorescence images of C-Dot-TPEA loaded-HeLa cells after exogenous Cu source treatment (100 μM CuCl$_2$) upon (C) 488 nm and (I) 800 nm excitation; (D, E) The fluorescence images of C-Dot-TPEA loaded-HeLa cells pretreated with 100 μM CuCl$_2$ for 1 h and then with (D) 50 μM Na$_2$S and (E) 100 μM Na$_2$S for 0.5 h ($\lambda_{ex}$=488 nm, the green fluorescence images were collected from 520 to 700 nm); (J, K) The fluorescence images of C-Dot-TPEA loaded-HeLa cells pretreated with 100 μM CuCl$_2$ for 1 h and then with (J) 50 μM Na$_2$S and (K) 100 μM Na$_2$S for 0.5 h ($\lambda_{ex}$=800 nm, the green fluorescence images were collected from 450 to 700 nm); (F, L) The mean fluorescence intensity of HeLa cells before and after the treatment (a, blank; b, 100 μM Cu$^{2+}$; c, 100 μM Cu$^{2+}$ and 50 μM Na$_2$S; d, 100 μM Cu$^{2+}$ and 100 μM Na$_2$S) upon (F) 488 nm and (L) 800 nm excitation. Scale bar: 30 μm. The mean intensity was generated from the analysis of five randomly selected fields of cells.
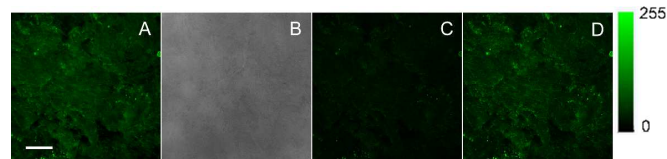


**Fig. 8** (A) Two-photon fluorescence and (B) bright-field images of lung cancer tissue slice stained with 0.2 mg mL$^{-1}$ C-Dot-TPEA for 6 h; (C, D)Two-photon fluorescence images of the C-Dot-TPEA-pretreated lung cancer tissue slice after its incubation with (C) 500 μM CuCl$_2$ and then with (D) 500 μM Na$_2$S. The fluorescence images were collected from 450 to700 nm with the excitation wavelength of 800 nm. The images shown are the representative images obtained at a depth of 150 μm with 40× magnification. Scale bar: 50 μm.

## Conclusions

In summary, a "turn-on" TPF sensor for H$_2$S has first been developed by using C-Dot as a two-photon fluorophore and designing TPEA-Cu$^{2+}$ complex as a specific receptor for H$_2$S. The present two-photon C-Dot-TPEA-Cu$^{2+}$ fluorescent sensor exhibits high selectivity and sensitivity, broad linear range, and low detection limit. Meanwhile, the C-Dot-based TPF probe shows long-wavelength excitation, excellent stability against light illumination and pH, good permeability, and low cytotoxicity. Accordingly, the nanohybridized TPF sensor with high analytical performance, as well as the remarkable properties of C-Dot, has successfully been applied for TPF imaging and biosensing of H$_2$S in live cells and tissues at the depth of 90–150 μm. This work has not only established a new approach to determination of H$_2$S in living system, but also provided a methodology to designing TPF sensors for thiols and other species, which may play critical roles in the biological and pathological events.

## Acknowledgements

## Notes and references

[a] Department of Chemistry, Tongji University, Shanghai 200092, China.

[b] Department of Chemistry, Shanghai Normal University, Shanghai 200234, China.

[c] Key Laboratory of Polar Materials and Devices, Ministry of Education, East China Normal University, Shanghai 200241, China.

[d] Department of Histology and Embryology, School of Medicine, Tongji University, Shanghai 200092, China.

† These authors contributed equally

Electronic Supplementary Information (ESI) available: NMR and MS spectra of AE-TPEA, apoptosis assay, and two-photon fluorescence microscopy images of RAW264.7 cells, HEK 293T cells and lung cancer tissue slice. See DOI: 10.1039/b000000x/

1    W. Denk, J. H. Strickler, W. W. Webb, *Science*, 1990, **248**, 73-76.

2    D. R. Larson, W. R. Zipfel, R. M. Williams, S. W. Clark, M. P. Bruchez, F. W. Wise, W. W. Webb, *Science*, 2003, **300**, 1434-1437.

*Analyst Accepted Manuscript*

3   S. C. Pu, M. J. Yang, C. C. Hsu, C. W. Lai, C. C. Hsieh, S. H. Lin, Y. M. Cheng, P. T. Chou, *Small*, 2006, **2**, 1308-1313.

4   H. M. Kim, B. R. Kim, J. H. Hong, J. S. Park, K. J. Lee, B. R. Cho, *Angew. Chem. Int. Ed.*, 2007, **46**, 7445-7448.

5   H. J. Kim, J. H. Han, M. K. Kim, C. S. Lim, H. M. Kim, B. R. Cho, *Angew. Chem. Int. Ed.*, 2010, **49**, 6786-6789.

6   L. Cao, X. Wang, M. J. Meziani, F. Lu, H. Wang, P. G. Luo, Y. Lin, B. A. Harruff, L. M. Veca, D. Murray, S. Y. Xie, Y. P. Sun, *J. Am. Chem. Soc.*, 2007, **129**, 11318-11319.

7   U. Resch-Genger, M. Grabolle, S. Cavaliere-Jaricot, R. Nitschke, T. Nann, *Nat. Methods*, 2008, **5**, 763-775.

8   S. T. Yang, X. Wang, H. Wang, F. Lu, P. G. Luo, L. Cao, M. J. Meziani, J. H. Liu, Y. Liu, M. Chen, Y. Huang, Y. P. Sun, *J. Phys. Chem. C*, 2009, **113**, 18110-18114.

9   S. T. Yang, L. Cao, P. G. Luo, F. Lu, X. Wang, H. Wang, M. J. Meziani, Y. Liu, G. Qi, Y. P. Sun, *J. Am. Chem. Soc.*, 2009, **131**, 11308-11309.

10  Y. P. Sun, X. Wang, F. Lu, L. Cao, M. J. Meziani, P. G. Luo, L. Gu, L. M. Veca, *J. Phys. Chem. C*, 2008, **112**, 18295-18298.

11  J. Zhou, Y. Yang, C. Zhang, *Chem. Commun.*, 2013, **49**, 8605-8607

12  A. Zhu, C. Ding, Y. Tian, Sci. Rep. 2013, 3, 2933.

13  T. Morita, M. A. Perrella, M. E. Lee, S. Kourembanas, *Proc. Natl. Acad. Sci. U.S.A.*, 1995, **92**, 1475-1479.

14  E. Culotta, D. E. Koshland, *Science*, 1992, **258**, 1862-1865.

15  G. Yang, L. Wu, B. Jiang, W. Yang, J. Qi, K. Cao, Q. Meng, A. K. Mustafa, W. Mu, S. Zhang, S. H. Snyder, R. Wang, *Science*, 2008, **322**, 587-590.

16  R. C. O. Zanardo, V. Brancaleone, E. Distrutti, S. Fiorucci, G. Cirino, J. L. Wallace, *FASEB J.*, 2006, **20**, 2118-2120.

17  G. Yang, L. Wu, R. Wang, *FASEB J.*, 2006, **20**, 553-555.

18  C. K. Nicholson, J. W. Calvert, *Pharmacol. Res.*, 2010, **62**, 289-297.

19  Y. J. Peng, J. Nanduri, G. Raghuraman, D. Souvannakitti, M. M. Gadalla, G. K. Kumar, S. H. Snyder, N. R. Prabhakar, *Proc. Natl. Acad. Sci. U.S.A.*, 2010, **107**, 10719-10724.

20  K. Eto, T. Asada, K. Arima, T. Makifuchi, H. Kimura, *Biochem. Bioph. Res. Co.*, 2002, **293**, 1485-1488.

21  P. Kamoun, *Med. Hypotheses*, 2001, **57**, 389-392.

22  M. Yusuf, B. T. Kwong Huat, A. Hsu, M. Whiteman, M. Bhatia, P. K. Moore, *Biochem. Bioph. Res. Co.*, 2005, **333**, 1146-1152.

23  E. Distrutti, A. Mencarelli, L. Santucci, B. Renga, S. Orlandi, A. Donini, V. Shah, S. Fiorucci, *Hepatology*, 2008, **47**, 659-667.

24  E. Fisher, *Chem. Ber.*, 1883, **16**, 2234-2236.

25  M. M. F. Choi, *Analyst*, 1998, **123**, 1631-1634.

26  D. Jimenez, R. Martinez-Manez, F. Sancenon, J. V. Ros-Lis, A. Benito, J. Soto, *J. Am. Chem. Soc.*, 2003, **125**, 9000-9001.

27  M. G. Choi, S. Cha, H. Lee, H. L. Jeon, S. K. Chang, *Chem. Commun.*, 2009, 7390-7392.

28  J. E. Doeller, T. S. Isbell, G. Benavides, J. Koenitzer, H. Patel, R. P. Patel, J. R. Lancaster, V. M. Darley-Usmar, D. W. Kraus, *Anal. Biochem.*, 2005, **341**, 40-51.

29  J. Radford-Knoery, G. A. Cutter, *Anal. Chem.*, 1993, **65**, 976-982.

30  H. Li, Y. Tian, Z. Deng, Y. Liang, *Analyst*, 2012, **137**, 4605-4609.

31  V. S. Lin, A. R. Lippert, C. J. Chang, *Proc. Natl. Acad. Sci. U.S.A.*, 2013, **110**, 7131-7135.

32  L. A. Montoya, M. D. Pluth, *Chem. Commun.*, 2012, **48**, 4767-4769.

33  C. Liu, J. Pan, S. Li, Y. Zhao, L. Y. Wu, C. E. Berkman, A. R. Whorton, M. Xian, *Angew. Chem. Int. Ed.*, 2011, **50**, 10327-10329.

34  X. Shen, C. B. Pattillo, S. Pardue, S. C. Bir, R. Wang, C. G. Kevil, *Free Rad. Biol. Med.*, 2011, **50**, 1021-1031.

35  C. Yu, X. Li, F. Zeng, F. Zheng, S. Wu, *Chem. Commun.*, 2013, **49**, 403-405.

36  K. Kawai, E. Matsutani, A. Maruyama, T. Majima, *J. Am. Chem. Soc.*, 2011, **133**, 15568-15577.

37  Q. Qu, A. Zhu, X. Shao, G. Shi, Y. Tian, *Chem. Commun.*, 2012, **48**, 5473-5475.

38  B. Kong, A. Zhu, C. Ding, X. Zhao, B. Li, Y. Tian, *Adv. Mater.*, 2012, **24**, 5844-5848.

39  A. Zhu, Q. Qu, X. Shao, B. Kong, Y. Tian, *Angew. Chem. Int. Ed.*, 2012, **51**, 7185-7189.

40  X. Shao, H. Gu, Z. Wang, X. Chai, Y. Tian, G. Shi, *Anal. Chem.*, 2012, **85**, 418-425.

41  A. Zhu, Y. Liu, Q. Rui, Y. Tian, *Chem. Commun.*, 2011, **47**, 4279-4281.

42  T. Tatsuma, S. Tachibana, A. Fujishima, *J. Phys. Chem. B*, 2001, **105**, 6987-6992.

43  J. M. Aubry, B. Cazin, *Inorg. Chem.*, 1988, **27**, 2013-2014.

44  H. Loertzer, S. Bauer, W. Moerke, P. Fornara, H. J. Broemme, *Transplant. Proc.*, 2006, **38**, 674-678.

45  M. H. Lim, D. Xu, S. J. Lippard, *Nat. Chem. Biol.*, 2006, **2**, 375-380.

46  J. Rosenthal, S. J. Lippard, *J. Am. Chem. Soc.*, 2010, **132**, 5536-5537.

47  H. Li, X. He, Z. Kang, H. Huang, Y. Liu, J. Liu, S. Lian, C. H. A. Tsang, X. Yang, S. T. Lee, *Angew. Chem. Int. Ed.*, 2010, **49**, 4430-4434.

48  O. Horner, J. J. Girerd, C. Philouze, L. Tchertanov, *Inorg. Chim. Acta*, 1999, **290**, 139-144.

49  C. Incarvito, M. Lam, B. Rhatigan, A. L. Rheingold, C. J. Qin, A. L. Gavrilova, B. Bosnich, *J. Chemical Soc., Dalton Trans.*, 2001, 3478-3488.

50  C. Hureau, G. Blondin, M. F. Charlot, C. Philouze, M. Nierlich, M. Cesario, E. Anxolabehere-Mallart, *Inorg. Chem.*, 2005, **44**, 3669-3683.

51  I. I. Ebralidze, G. Leitus, L. J. W. Shimon, R. Neumann, *J. Mol. Struct.*, 2008, **891**, 491-497.

52  S. K. Bae, C. H. Heo, D. J. Choi, D. Sen, E. H. Joe, B. R. Cho, H. M. Kim, *J. Am. Chem. Soc.*, 2013, **135**, 9915-9923.

53  K. Sasakura, K. Hanaoka, N. Shibuya, Y. Mikami, Y. Kimura, T. Komatsu, T. Ueno, T. Terai, H. Kimura, T. Nagano, *J. Am. Chem. Soc.*, 2011, **133**, 18003-18005.

54  A. R. Lippert, E. J. New, C. J. Chang, *J. Am. Chem. Soc.*, 2011, **133**, 10078-10080.

55  S. Chen, Z. Chen, W. Ren, H. Ai, *J. Am. Chem. Soc.*, 2012, **134**, 9589-9592.

56  H. Peng, Y. Cheng, C. Dai, A. L. King, B. L. Predmore, D. J. Lefer, B. Wang, *Angew. Chem. Int. Ed.*, 2011, **50**, 9672-9675.

57  Y. Chen, C. Zhu, Z. Yang, J. Chen, Y. He, Y. Jiao, W. He, L. Qiu, J. Cen, Z. Guo, *Angew. Chem. Int. Ed.*, 2013, **52**, 1688-1691.

58  C. Li, M. Yu, Y. Sun, Y. Wu, C. Huang, F. Li, *J. Am. Chem. Soc.*, 2011, **133**, 11231-11239.

**Analyst Accepted Manuscript**

## Entry for the Table of Contents
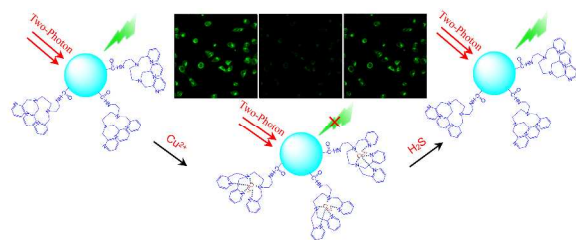


A "turn-on" two-photon fluorescent sensor for $H_2S$ is developed, in which C-Dot is employed as a two-photon fluorophore and AE-TPEA-$Cu^{2+}$ complex is first designed as a specific receptor for $H_2S$.

**Analyst Accepted Manuscript**